Deterministic Boltzmann Transport Equation Solver: Validation and Heat Generation Modeling

Ethan Kao*†‡, Christoph Jungemann§, Michel Houssa†‡, Stanislav Tyaginov‡
*Ethan.Kao@imec.be, †KU Leuven, Belgium, ‡imec, Leuven, Belgium, §RWTH Aachen, Germany

***Abstract*—The heat generation rate is commonly calculated via phonon energy transfer rate. To ensure consistency with the energy balance equation, we reformulate the heat generation rate based on the carrier energy loss and demonstrate the equivalence of both approaches. The deterministic Boltzmann Transport Equation (BTE) solver is validated under low-field conditions using the distribution function and the mobility derived from the relaxation time approximation. Additionally, we introduce an approximation to address a non-removable singularity in the mobility calculation. These results demonstrate the potential of the deterministic BTE solver for predictive simulations of self-heating effects and hot-carrier degradation in advanced semiconductor devices.**

***Index Terms*—validation, heat generation, carrier transport, mobility, spherical harmonics expansion, conservation of energy**

I. Introduction

As field-effect-transistors (FETs) scale down, the self-heating effect becomes increasingly significant [1]. Accurate simulation of this detrimental phenomenon — as it was demonstrated by Pop *et al.* [2] by solving the Boltzmann transport equation (BTE) with the Monte Carlo (MC) approach — should be based on the phonon transfer rate, not Joule heating. Another phenomenon detrimental to transistor performance and intimately related to carrier transport is hot-carrier degradation (HCD), often accelerated by self-heating [3], [4]. Precise modeling of HCD requires computation of the high-energy tail of the carrier energy distribution function [5], [6]. However, the transient nature of the MC technique results in a long CPU time to obtain an accurate high-energy tail, making the deterministic BTE (D-BTE) solver essential.

To cover these two reliability concerns, we develop ***imec*SHE**, a D-BTE solver using the *spherical harmonics expansions* (SHE) method, based on the open-source BTE solver **ViennaSHE** [7], [8]. Previous studies towards carrier and phonon transport based on D-BTE solvers included heat generation modeling of HBTs via the phonon energy transfer perspective [9], [10]. Here, we approach this problem from the carrier kinetic energy perspective and demonstrate these two paradigms using a silicon $n^+/n/n^+$ structure. As the second important goal of our work, we provide a procedure to validate the D-BTE solver.

II. Models and Assumptions

The steady-state single-valley bipolar BTE is solved assuming identical distribution functions across equivalent valleys. To reduce the computational time, the SHE order is set to 1. The Pauli principle is neglected due to its negligible impact on the DC characteristics [11] of the bulk silicon for *imec*SHE validation and the $n^+/n/n^+$ structure for heat generation modeling. Scattering mechanisms, including acoustic phonon, optical phonon, and impurity scattering are treated as isotropic.

III. Validation

To validate *imec*SHE, a 100-nm silicon slab is used. We first compare SHE coefficients $f_{l,m}(\boldsymbol{r},\varepsilon)$ of the distribution function $f(\boldsymbol{r},\boldsymbol{k})$ against the results obtained with the *microscopic relaxation time approximation* (RTA) [12]. Next, we validate the low-field carrier transport by comparing carrier mobility vs. its analytical formulas, for which we circumvent a non-removable singularity by an approximation we proposed. Validation parameters are summarized in Table I.

TABLE I
Parameters of Si used for calculations.

	Validation	Calibration	
Quantity	Electron	Electron	Hole
α (eV^{-1})	0.0 [13]	0.5 [14]	0.935 [15]
m_t/m_0	0.295 [13]	0.19 [16]	1.15247 [17]
m_l/m_0	0.295 [13]	0.98 [16]	1.15247 [17]
E_1 (eV)	9.0 [13]	7.5 (5.0 [18])	3.00 (2.2 [19])
D_tK (GeV·cm^{-1})	0.8 [13]	0.55 (0.55 [18])	0.425 (0.50 [19])
$\hbar\omega_{\text{op}}$ (meV)	38.8 [13]	25.0 (42.6 [18])	62.0 (63.3 [19])

Note: α is the nonparabolicity factor; m_t, m_l are transverse and longitudinal effective masses; E_1 and D_tK are deformation potentials for acoustic and optical phonon scattering, respectively; $\hbar\omega_{\text{op}}$ is the optical phonon energy.

A. Distribution Function

Based on the RTA and the isotropic scattering approximation [12], one can obtain the SHE coefficients of the distribution function in a uniform electric field $\boldsymbol{E}$:

$$f_{l,m}(\varepsilon) = f^{\text{eq}}(\varepsilon)\left[\frac{\delta_{l,0}\delta_{m,0}}{Y^{0,0}} \pm \frac{e\tau(\varepsilon)v(\varepsilon)}{Y^{0,0}k_BT}\boldsymbol{a}_{0,0}^{l,m\,\mathrm{T}}\mathbf{T}^{\mathrm{T}}\boldsymbol{E}\right], \quad (1)$$

where the upper (lower) sign is for holes (electrons), $Y^{0,0}$ the zeroth order spherical harmonics, ε the carrier kinetic energy, $\tau(\varepsilon)$ the relaxation time, $v(\varepsilon)$ the carrier velocity, $\boldsymbol{a}_{0,0}^{l,m}$ the coupling coefficient defined in [20], $\mathbf{T}$ the Herring-Vogt transform matrix [21], and $f^{\text{eq}}(\varepsilon)$ the Maxwell-Boltzmann distribution function.

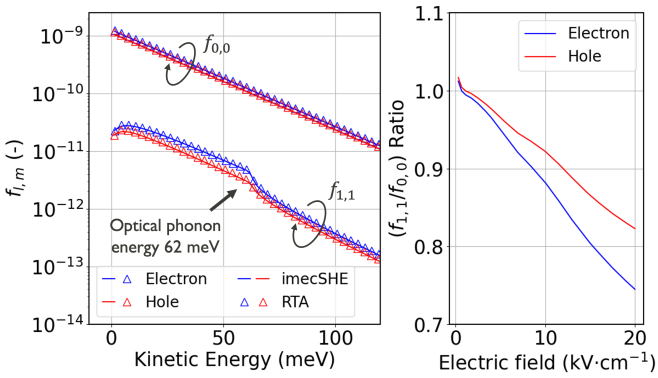

Fig. 1. The RTA validation results.

Fig. 1 compares the numerical result of *imec*SHE and the theoretical result obtained with the RTA. Only $f_{0,0}(\varepsilon)$ and $f_{1,1}(\varepsilon)$ are considered because the electric field is along the x-axis. One can see that these results are in good agreement and the average numerical-to-theoretical $\langle f_{1,1}(\varepsilon)\rangle_\varepsilon / \langle f_{0,0}(\varepsilon)\rangle_\varepsilon$ ratio gradually deviates from 1 as expected. Therefore, we can conclude that *imec*SHE can properly reproduce the theoretical carrier energy distribution function.

B. Mobility Calculation and Singularity Treatment

Typically, the carrier mobility is calculated using the current density, $\mu_{ij} = J_i/(neE_j)$, but this approach does not allow for analyzing contributions from individual scattering mechanisms. Therefore, we adopt the RTA-based mobility tensor [20]. Using the SHE of the distribution function,

$$f(\boldsymbol{r},\boldsymbol{k}) = \sum_{l=0}^{\infty}\sum_{m=-l}^{l} f_{l,m}(\boldsymbol{r},\varepsilon)Y^{l,m}(\theta,\phi), \tag{2}$$

the mobility tensor $\boldsymbol{\mu}(\boldsymbol{r})$ is given by:

$$\boldsymbol{\mu}(\boldsymbol{r}) = \int_0^\infty \boldsymbol{\mu}(\boldsymbol{r},\varepsilon)\, d\varepsilon. \tag{3}$$

Here, the spectral mobility tensor $\boldsymbol{\mu}(\boldsymbol{r},\varepsilon)$ is defined as

$$\begin{aligned}\boldsymbol{\mu}(\boldsymbol{r},\varepsilon) \coloneqq{}& \frac{e}{nm_0 Y^{0,0}}\mathbf{T}^2\tau(\varepsilon)f_{0,0}(\boldsymbol{r},\varepsilon)\,Z(\varepsilon)\\ &+\frac{e}{n}\sum_{l=0}^{\infty}\sum_{m=-l}^{l}\mathbf{T}\mathbf{S}_k^{l,m}\mathbf{T}^{\mathrm{T}}v^2(\varepsilon)\frac{d\tau}{d\varepsilon}f_{l,m}(\boldsymbol{r},\varepsilon)\,Z(\varepsilon),\end{aligned} \tag{4}$$

where $Z(\varepsilon)$ is the reduced two-spin density of states [20] and $\mathbf{S}_k^{l,m}$ is the coupling matrix defined as

$$\begin{aligned}\mathbf{S}_k^{l,m} \coloneqq{}& \int_\Omega \boldsymbol{e}_k\boldsymbol{e}_k^{\mathrm{T}}Y^{l,m}d\Omega = \frac{\delta_{l,0}\delta_{m,0}}{3Y^{0,0}}\mathbf{I} + \frac{\delta_{l,2}}{6\sqrt{5\pi}\,(Y^{0,0})^2}\\ &\times\left[-\delta_{m,0}\mathbf{I}+\sqrt{3}\begin{pmatrix}\delta_{m,2} & \delta_{m,-2} & \delta_{m,1}\\ \delta_{m,-2} & -\delta_{m,2} & \delta_{m,-1}\\ \delta_{m,1} & \delta_{m,-1} & \sqrt{3}\delta_{m,0}\end{pmatrix}\right].\end{aligned} \tag{5}$$

However, from the isotropic relaxation time [12],

$$\tau(\varepsilon) = \left[\frac{2\pi}{N_{\mathrm{e}}}\sum_\eta \sigma_\eta(\varepsilon)Z(\varepsilon+\Delta\varepsilon_\eta)\right]^{-1}, \tag{6}$$

where N_{e} is the number of equivalent valleys and $\sigma_\eta(\varepsilon)$ is the isotropic transition rate of the mechanism η, one can see that $d\tau/d\varepsilon$ in Eq. (4) introduces two singularities due to the Dirac δ-function model in the *Fermi's golden rule*. One of them is removable due to elastic scattering with $\Delta\varepsilon_\eta = 0$ and can be regularized by combining v^2 with $dZ/d\varepsilon$. The other is non-removable due to the inelastic optical phonon scattering with $\Delta\varepsilon_\eta = -\hbar\omega_\eta$. We observe that the mobility follows the form

$$\mu = \int_{\hbar\omega_\eta}^\infty \frac{g(\varepsilon)}{\sqrt{\varepsilon-\hbar\omega_\eta}}d\varepsilon + C, \tag{7}$$

where both $g(\varepsilon)$ and C stand for non-singular terms. Therefore, numerical integration overestimates or underestimates the mobility depending on grid placement relative to the singularity $\varepsilon = \hbar\omega_\eta$. To mitigate the numerical impact of this singularity, we assume that $g(\varepsilon)$ varies slowly in the vicinity of $\varepsilon = \hbar\omega_\eta$ and that the lowest node value above $\hbar\omega_\eta$ on the energy grid is $\hbar\omega_\eta + \xi$. The integral in Eq. (7) near the singularity can thus be approximated as

$$\int_{\hbar\omega_\eta}^{\hbar\omega_\eta+\xi}\frac{g(\varepsilon)}{\sqrt{\varepsilon-\hbar\omega_\eta}}d\varepsilon \approx 2g\left(\hbar\omega_\eta+\frac{\xi}{2}\right)\sqrt{\xi}, \tag{8}$$

where $g(\varepsilon)$ is approximated as $g(\hbar\omega_\eta + \xi/2)$ when ξ is sufficiently small, thereby making the singularity integrable.

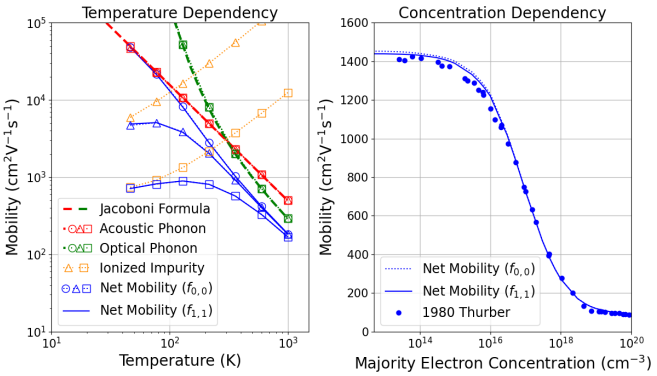

Fig. 2. Electron mobility as a function of temperature and doping concentration at 0.3 kV·cm^{-1}, calculated using validation parameters listed in Table I. Markers ○, □, Δ represents donor concentrations of 0/10^{16}/1.3 × 10^{17} cm^{-3}, respectively.

Fig. 2 shows that *imec*SHE reproduces the analytical [13] and experimental mobility [22] curves with good accuracy. We employ two approaches for mobility calculations. The first approach evaluates the mobility from the current density via $f_{1,1}(\varepsilon)$ [20]. As for the second one, it relies on the RTA and the mobility is calculated via $f_{0,0}(\varepsilon)$ as shown in Eq. (4). One can see that the mobilities calculated from $f_{0,0}(\varepsilon)$ and $f_{1,1}(\varepsilon)$ are identical. The left plot highlights the consistency of *imec*SHE results with the theoretical predictions for phonon-limited mobilities obtained by Jacoboni [13]. Because analytical models for impurity scattering mobility involve approximations [13], *imec*SHE's results are compared with the experimental data [22], as shown in the right plot of Fig. 2. However, an empirical correction factor $\zeta(N_{\mathrm{A}}, N_{\mathrm{D}})$ for the impurity scattering

rate is necessary, $S^{\mathrm{CBH}}\left(\boldsymbol{k},\boldsymbol{k}'\right) = \zeta\left(N_{\mathrm{A}},N_{\mathrm{D}}\right)S^{\mathrm{BH}}\left(\boldsymbol{k},\boldsymbol{k}'\right)$, because the Brooks-Herring model assumes long screening lengths valid only for low doping concentrations [12], [23].

IV. Calibration

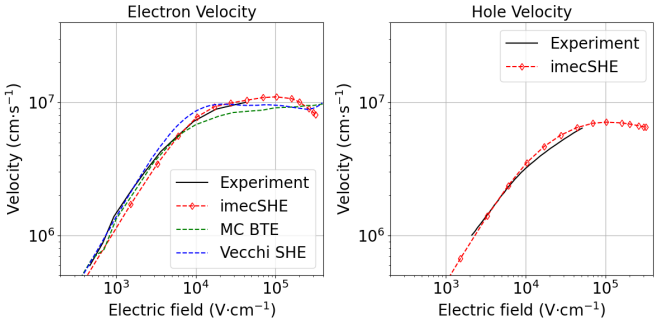

Fig. 3. Comparison of the carrier velocity calculated using *imec*SHE with results from stochastic MC BTE [24], deterministic BTE [18], and experimental measurements [19], [25]. Parameter values obtained with the calibration procedure are summarized in Table I.

To calibrate *imec*SHE, we use a 100-nm slab of undoped silicon with $\langle 111\rangle$ orientation. The full-band density of states (DOS) [14] is used for electrons, but the effective mass is retained for the Herring-Vogt transform [14] and the hole DOS [15]. Fig. 3 depicts good agreement between velocity calculated with calibrated *imec*SHE, the experimental data [19], [25], and the results of both stochastic [24] and deterministic [18] BTE solvers. The decay of the mobility above 100 kV·cm^{-1} in Fig. 3 is presumably related to the enhancement of scattering. Key parameters are summarized in Table. I, where the acoustic and the optical phonon scattering parameters are comparable with values reported in the literature [18], [19].

V. Heat Generation Modeling

A. Validation against Conservation of Energy

We begin with the energy balance equation [26]:

$$\frac{\partial u}{\partial t} = \boldsymbol{J}\cdot\boldsymbol{E} - \nabla\cdot\boldsymbol{J}_u - R, \tag{9}$$

where $\boldsymbol{J}$, $\boldsymbol{J}_u$, and $R \coloneqq -\frac{2}{\Omega_s}\left(\frac{\partial f}{\partial t}\right)_{\mathrm{coll}}$ are the current density, the energy current density, and the carrier kinetic energy loss rate, respectively. Since phonons absorb the energy lost by carriers, R is the *actual* heat generation rate. Assuming isotropic scattering and neglecting the Pauli principle, the heat generation rate R can be derived as

$$R = \frac{N_e}{\left(Y^{0,0}\right)^3}\sum_{\eta=0}^{1}\int_0^{\infty}\left[\sigma\left(\varepsilon,\varepsilon+\varepsilon_\eta\right)f_{0,0}(\varepsilon)Z\left(\varepsilon+\varepsilon_\eta\right)\right. \\ \left. - \sigma\left(\varepsilon-\varepsilon_\eta,\varepsilon\right)f_{0,0}\left(\varepsilon-\varepsilon_\eta\right)Z\left(\varepsilon-\varepsilon_\eta\right)\right]Z(\varepsilon)\varepsilon d\varepsilon, \tag{10}$$

where $\varepsilon_0 = \hbar\omega$ ($\varepsilon_1 = -\hbar\omega$) is the change of the carrier kinetic energy due to phonon capture (emission). If the Pauli principle is considered, the first and the second term within the bracket needs to be multiplied with an additional factor of $1 - f_{0,0}(\varepsilon+\varepsilon_\eta)Y^{0,0}$ and $1 - f_{0,0}(\varepsilon)Y^{0,0}$, respectively.

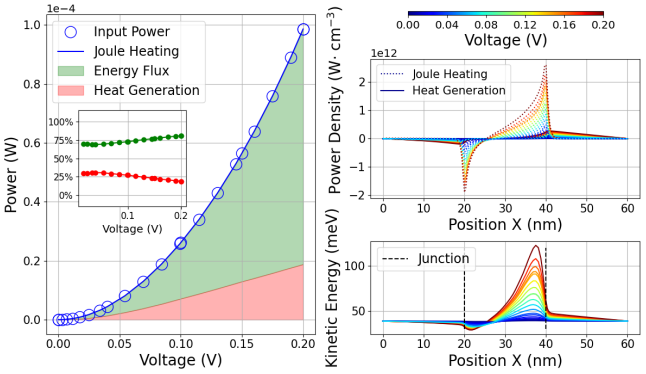

Fig. 4. Power components (left), heat generation (top right), and kinetic energy (bottom right) profiles of a silicon $n^+/n/n^+$ structure with donor concentrations of $10^{20}/10^{16}/10^{20}$ cm^{-3}.

Fig. 4 presents the steady-state volume-integrated energy terms from Eq. (9) for a silicon $n^+/n/n^+$ device ($10^{20}/10^{16}/10^{20}$ cm^{-3}). The left plot validates *imec*SHE's consistency via $IV = \iiint \boldsymbol{J}\cdot\boldsymbol{E}d\boldsymbol{r}^3$, matching the input power with the Joule heating. The equality between the input power and the sum of the energy flux density and the heat generation verifies energy conservation in the electron system. The energy flux density is computed independently. The inset of the left plot shows that less than 30% of input power converts to phonon energy. The top-right plot shows that most heat is generated in the drain, where electrons have enough energy to emit optical phonons (see bottom-right plot). Despite higher kinetic energy in the channel, the much lower electron density ($\sim 10^4$ times smaller than in the drain) results in heat generation comparable to that in the drain.

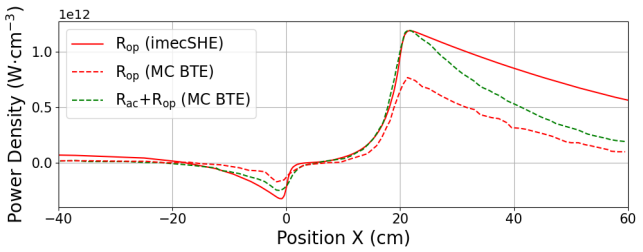

Fig. 5. Power density due to heat generation under 0.6 V calculated with *imec*SHE (with parameters parameters summarized in Table I) and that obtained by Pop *et al.* [27] with an MC BTE solver. The silicon $n^+/n/n^+$ structure consists of source, channel, and drain regions with lengths of 100/20/100 nm and donor concentrations of $10^{18}/10^{16}/10^{18}$ cm^{-3}, respectively.

B. Equivalence of two interpretations of the heat generation

The heat generation rate in Eq. (10) apparently differs from the one below commonly used in MC BTE solvers [2]:

$$R = \hbar\omega\left(S^{\mathrm{out,emission}} - S^{\mathrm{out,capture}}\right) \\ = \hbar\omega\left(S^{\mathrm{in,emission}} - S^{\mathrm{in,capture}}\right), \tag{11}$$

where S is the macroscopic intravalley scattering rate. Eq. (10) and Eq. (11) correspond to carrier and phonon centric ap-

proaches to calculation of the heat generation rate, respectively. The equivalence between Eq. (10) and Eq. (11) can be easily shown by a change of variable in Eq. (10), substituting $\varepsilon = \varepsilon^* + \hbar\omega$, so that the kinetic energy remains positive for the DOS $Z(\varepsilon^*)$. The same method applies to anisotropic scattering, with the additional step of projecting the scattering rate onto spherical harmonics.

C. Validation against stochastic MC BTE solver

Fig. 5 compares the heat generation rates calculated with *imec*SHE and by Pop *et al.* [27]. The discrepancy between the heat generation rates due to inelastic optical phonon scattering (red lines) appears quite reasonable because the model of Pop assumes 50.0 meV for optical phonon enenrgy, while *imec*SHE uses 38.8 meV (Table I). Despite different parameters used in these two transport simulators, the overall profiles are comparable, thereby validating consistency of heat generation modeling with *imec*SHE. The close agreement between the rate R_{op} calculated with *imec*SHE and $R_{\text{ac}} + R_{\text{op}}$ obtained by Pop *et al.* within the channel demonstrates the validity of *imec*SHE for heat generation modeling.

VI. Conclusions

We present a deterministic Boltzmann transport equation (D-BTE) solver *imec*SHE validated against simulation results and experimental data. The validation procedure ensures that *imec*SHE is capable of accurately modeling the low-field transport and heat generation in Si-based devices. This procedure and the derived formulas should be of interest for the community as they provide clear methodology for validating D-BTE solvers. The equivalence between carrier and phonon interpretations of heat generation is also demonstrated, thereby ensuring that either interpretations can be employed.

Acknowledgment

The authors are thankful to Drs. A. Makarov, G. Doornbos, and Z. Stanojević for insightful discussions. We would also like to express our sincere gratitude to Dr. K. Rupp for his invaluable contributions to the ViennaSHE development.

References

[1] C. Prasad, "A review of self-heating effects in advanced CMOS technologies," *IEEE Transactions on Electron Devices*, vol. 66, no. 11, pp. 4546–4555, 2019.

[2] E. Pop, "Energy dissipation and transport in nanoscale devices," *Nano Research*, vol. 3, pp. 147–169, 2010.

[3] C. Prasad, S. Ramey, and L. Jiang, "Self-heating in advanced CMOS technologies," in *2017 IEEE International Reliability Physics Symposium (IRPS)*. IEEE, 2017, pp. 6A–4.

[4] A. Rahman, J. Dacuna, P. Nayak, G. Leatherman, and S. Ramey, "Reliability studies of a 10nm high-performance and low-power CMOS technology featuring 3rd generation FinFET and 5th generation HK/MG," in *2018 IEEE International Reliability Physics Symposium (IRPS)*. IEEE, 2018, pp. 6F–4.

[5] M. Bina, K. Rupp, S. Tyaginov, O. Triebl, and T. Grasser, "Modeling of hot carrier degradation using a spherical harmonics expansion of the bipolar Boltzmann transport equation," in *2012 International Electron Devices Meeting*. IEEE, 2012, pp. 30–5.

[6] S. Tyaginov, M. Bina, J. Franco, D. Osintsev, O. Triebl, B. Kaczer, and T. Grasser, "Physical modeling of hot-carrier degradation for short- and long-channel MOSFETs," in *2014 IEEE International Reliability Physics Symposium*. IEEE, 2014, pp. XT–16.

[7] K. Rupp, "ViennaSHE: An open-source project on SourceForge," https://viennashe.sourceforge.net/, 2022, development of *imec*SHE was initiated from the version 1.1.1 of ViennaSHE, which employed a vertex-based finite-volume scheme, rather than from the current version available online.

[8] K. Rupp, C. Jungemann, S.-M. Hong, M. Bina, T. Grasser, and A. Jüngel, "A review of recent advances in the spherical harmonics expansion method for semiconductor device simulation," *Journal of computational electronics*, vol. 15, pp. 939–958, 2016.

[9] H. Kamrani, T. Kochubey, D. Jabs, and C. Jungemann, "Electrothermal simulation of SiGe HBTs and investigation of experimental extraction methods for junction temperature," in *2015 International Conference on Simulation of Semiconductor Processes and Devices (SISPAD)*. IEEE, 2015, pp. 108–111.

[10] H. Kamrani, D. Jabs, V. dAlessandro, N. Rinaldi, K. Aufinger, and C. Jungemann, "A deterministic and self-consistent solver for the coupled carrier-phonon system in SiGe HBTs," *IEEE Transactions on Electron Devices*, vol. 64, no. 2, pp. 361–367, 2017.

[11] S.-M. Hong and C. Jungemann, "Inclusion of the Pauli principle in a deterministic Boltzmann equation solver based on a spherical harmonics expansion," *Journal of computational electronics*, vol. 9, no. 3, pp. 153–159, 2010.

[12] C. Jungemann and B. Meinerzhagen, *Hierarchical Device Simulation: The Monte-Carlo Perspective*. Springer Science & Business Media, 2003.

[13] C. Jacoboni, *Theory of electron transport in semiconductors: a pathway from elementary physics to nonequilibrium Green functions*. Springer Science & Business Media, 2010, vol. 165.

[14] S. Jin, S.-M. Hong, and C. Jungemann, "An efficient approach to include full-band effects in deterministic Boltzmann equation solver based on high-order spherical harmonics expansion," *IEEE Transactions on Electron Devices*, vol. 58, no. 5, pp. 1287–1294, 2011.

[15] T. Kunikiyo, M. Takenaka, M. Morifuji, K. Taniguchi, and C. Hamaguchi, "A model of impact ionization due to the primary hole in silicon for a full band Monte Carlo simulation," *Journal of applied physics*, vol. 79, no. 10, pp. 7718–7725, 1996.

[16] C. Jacoboni and L. Reggiani, "Bulk hot-electron properties of cubic semiconductors," *Advances in Physics*, vol. 28, no. 4, pp. 493–553, 1979.

[17] J. E. Lang, F. L. Madarasz, and P. M. Hemenger, "Temperature dependent density of states effective mass in nonparabolic p-type silicon," *Journal of applied physics*, vol. 54, no. 6, pp. 3612–3612, 1983.

[18] M. C. Vecchi and M. Rudan, "Modeling electron and hole transport with full-band structure effects by means of the spherical-harmonics expansion of the BTE," *IEEE Transactions on Electron Devices*, vol. 45, no. 1, pp. 230–238, 2002.

[19] G. Ottaviani, L. Reggiani, C. Canali, F. Nava, and A. Alberigi-Quaranta, "Hole drift velocity in silicon," *Physical Review B*, vol. 12, no. 8, p. 3318, 1975.

[20] M. Rudan, R. Brunetti, S. Reggiani *et al.*, *Springer Handbook of Semiconductor Devices*. Springer, 2023.

[21] N. Goldsman, L. Henrickson, and J. Frey, "A physics-based analytical/numerical solution to the Boltzmann transport equation for use in device simulation," *Solid-state electronics*, vol. 34, no. 4, pp. 389–396, 1991.

[22] W. Thurber, R. Mattis, Y. Liu, and J. Filliben, "Resistivity-dopant density relationship for phosphorus-doped silicon," *Journal of the Electrochemical Society*, vol. 127, no. 8, p. 1807, 1980.

[23] D. Chattopadhyay and H. Queisser, "Electron scattering by ionized impurities in semiconductors," *Reviews of Modern Physics*, vol. 53, no. 4, p. 745, 1981.

[24] M. V. Fischetti and S. E. Laux, "Monte Carlo analysis of electron transport in small semiconductor devices including band-structure and space-charge effects," *Physical Review B*, vol. 38, no. 14, p. 9721, 1988.

[25] C. Canali, C. Jacoboni, F. Nava, G. Ottaviani, and A. Alberigi-Quaranta, "Electron drift velocity in silicon," *Physical Review B*, vol. 12, no. 6, p. 2265, 1975.

[26] A. C. Smith, J. F. Janak, and R. B. Adler, *Electronic conduction in solids*. McGraw Hill, 1967.

[27] E. Pop, J. Rowlette, R. Dutton, and K. Goodson, "Joule heating under quasi-ballistic transport conditions in bulk and strained silicon devices," in *2005 International Conference On Simulation of Semiconductor Processes and Devices*. IEEE, 2005, pp. 307–310.